Tomographic Measurement of Local Cerebral Glucose Metabolic Rate in Humans with (F-18)2-Fluoro-2-Deoxy-D-Glucose: Validation of Method

M. E. Phelps, PhD, S. C. Huang, DSc, E. J. Hoffman, PhD, C. Selin, MS, L. Sokoloff, MD, and D. E. Kuhl, MD

Tracer techniques and quantitative autoradiographic and tissue counting models for measurement of metabolic rates were combined with positron computed tomography (PCT) and (F-18)2-fluoro-2-deoxy-D-glucose (FDG) for the measurement of local cerebral metabolic rate for glucose (LCMRGlc) in humans. A three-compartment model, which incorporates hydrolysis of FDG-6-PO_4 to FDG, was developed for the measure of kinetic constants and calculation of LCMRGlc. Our model is an extension of that developed by Sokoloff et al. Although small, hydrolysis of FDG-6-PO_4 was found to be significant. A PCT system, the ECAT, was used to determine the rate constants, lumped constant, and stability of the model in human beings. The data indicate that cerebral FDG-6-PO_4 in humans increases for about 90 minutes, plateaus, and then slowly decreases. After 10 minutes, cerebral blood FDG activity levels were found to be a minor fraction of tissue activity. Precursor pool turnover rate, distribution volumes, and red blood cell–plasma concentration ratios were determined. Reproducibility (precision) of LCMRGlc measurements (~2 cm^2 regions) was ± 5.5% over a 5-hour period. The replacement of arterial blood sampling with venous sampling was validated.

Phelps ME, Huang SC, Hoffman EJ, et al: Tomographic measurement of local cerebral glucose metabolic rate in humans with (F-18)2-fluoro-2-deoxy-D-glucose: validation of method. Ann Neurol 6:371–388, 1979

Quantitative autoradiography and tissue counting techniques used with compounds labeled with radioactive isotopes have been a source of much of the present knowledge of physiological processes. We have combined the principles of these techniques with positron computed tomography (PCT) [36] to perform the equivalent of quantitative autoradiography in vivo. We call this method physiological tomography (PT) [39, 41]. The objective of PT is to use the tracer method in human beings and animals for in vivo study of physiological processes.

PT requires: (1) labeled compounds which not only trace a physiological process but also behave in such a manner that they can be analytically modeled, (2) physiological models that are appropriately formulated and validated to derive physiological variables of interest from PCT data, and (3) an imaging system that is capable of performing quantitative measurements of tissue radioactivity concentrations and is also well characterized in terms of resolution, sensitivity, and signal-to-noise ratios in the image. Here we describe the development and validation of the PT approach to the measurement of local cerebral metabolic rate for glucose (CMRGlc) with (F-18)2-fluoro-2-deoxy-D-glucose (FDG) in humans.

The model for this technique is based upon the autoradiographic model for measurement of local CMRGlc with (C-14)deoxyglucose (DG) developed by Sokoloff et al [53]. After Ido and co-workers [24] developed a synthesis for FDG, Reivich [48, 49], Kuhl [28], and Phelps [39] and their associates applied Sokoloff's model with emission computed tomography (ECT) to the measurement of CMRGlc with FDG in human volunteers. Kuhl et al [29, 30] have also used FDG and PCT to study patients with stroke and epilepsy. A model for the in vivo mea-

From the Division of Nuclear Medicine, UCLA School of Medicine, the Laboratory of Nuclear Medicine and Radiation Biology, University of California, Los Angeles, CA, and the Laboratory of Cerebral Metabolism, National Institutes of Health, Bethesda, MD.

Accepted for publication Apr 13, 1979.

Address reprint requests to Dr Phelps, Division of Nuclear Medicine, Department of Radiological Sciences, UCLA School of Medicine, Los Angeles, CA 90024.

surement of CMRGlc developed by Raichle et al [46] with (C-11)glucose has been used with a single-detector technique [46] and with PCT [47] to measure global CMRGlc in the rhesus monkey. Although this method has been utilized only for whole-brain measurements of CMRGlc, it should also be applicable to regional measurements with PCT.

DG and FDG are glucose analogs which compete with glucose for facilitated transport sites and with hexokinase for phosphorylation to DG- or FDG-6-phosphate. An advantage of this analog over labeled glucose is that the end-product of phosphorylation (DG- or FDG-6-PO_4) is trapped in the tissue and released with a very slow clearance. This is because DG- or FDG-6-PO_4 cannot be metabolized further [53], DG- or FDG-6-PO_4 has a low membrane permeability, and glucose-6-phosphatase (which can hydrolyze the 6-PO_4 form to DG or FDG) exhibits low activity levels in brain [20, 21, 44, 45]. This trapping mechanism provides an excellent means for development and application of analytical models for the measurement of CMRGlc with PCT.

Like DG, FDG has been shown by Bessell et al [5] and Reivich et al [48, 49] to be a good substrate for yeast hexokinase, and FDG-6-PO_4 has been identified as the end-product of cerebral metabolism in the mouse by Gallagher et al [12]. FDG has been observed to concentrate in the brain of rat, mouse, and dog [11, 12], man [28, 30, 39, 43, 48, 49] and dog, monkey, and man [42]. Gallagher et al [12] have shown that FDG is rapidly converted to FDG-6-PO_4 in mouse brain and that the total radioactivity remains reasonably constant for about an hour, then slowly decreases. Phelps et al [42, 43] have observed in humans that after injection of FDG, the brain F-18 activity level steadily increases for about 1½ hours and then slowly decreases. Reivich et al [48, 49] and Kuhl et al [28] used the model of Sokoloff et al [53] with the rate constants for DG in rats to measure the local CMRGlc in 2 human volunteers by ECT. Their measured values of CMRGlc for whole brain are in good agreement with published values obtained by the Fick method in humans, and their local values are in conformity with measurements in corresponding structures of the brain of the rhesus monkey [49].

All these data indicate that FDG is a suitable glucose analog for measuring CMRGlc. However, no one has yet measured the rate constants and lumped constant (LC) for FDG in any animal, and DG values are known only for the rat [53] and monkey [26]. Studies have not yet been carried out to determine the rate of hydrolysis of FDG-6-PO_4 to FDG, and, if it is significant, to incorporate this process into the compartmental model. The reproducibility of reported measurements and precision of the FDG method for measuring CMRGlc also have not been determined.

Recently, Hawkins and Miller [19] have challenged whether DG, as applied by Sokoloff et al [53], can be used for the quantitative measure of CMRGlc and assert that Sokoloff's model is not quantitative because DG-6-PO_4 is rapidly hydrolyzed to DG that clears from the tissue. This would be consistent with low values of CMRGlc with the DG method; however, the values obtained with this model are at least as high as the values expected from measurements of the brain as a whole [53].

In this work we have used a three-compartment model developed in our laboratory by Huang et al [23] and the ECAT positron tomograph [40] (ORTEC, Inc, Life Sciences Division, Oak Ridge, TN) to measure the rate constants of the model for FDG in humans. Our three-compartment model for CMRGlc includes hydrolysis of FDG-6-PO_4 to FDG and is an extension of the Sokoloff model. We have estimated the LC of FDG and have measured the stability and precision of the tomographic measurement of local CMRGlc from 0 to 5 hours after injection. The time courses of free FDG in plasma and tissue and FDG-6-PO_4 in tissue have been examined along with the ratio of red blood cell to plasma activity in humans. Studies in dog, monkey, and man were performed to investigate the replacement of arterial blood sampling employed by Sokoloff et al [53] and Reivich et al [48, 49] by venous sampling of a resting arm or hand. Venous sampling has been further studied by sampling blood from a hand heated to about 44°C to "arterialize" the venous blood. Studies were also carried out to determine how well this technique can delineate the internal substructures of the brain.

The model has been incorporated into the system software of the ECAT and a protocol established to allow this PT technique to be used in an automated manner by a nuclear medicine technician in a research or clinical environment.

Material and Methods

Preparation of FDG

FDG with specific activities of 20 to 30 mCi per milligram was synthesized by the method of Ido and colleagues [24, 50]. The radiochemical purity, as assayed by high-pressure liquid chromatography, was greater than 95%; the remainder was determined by thin-layer chromatography to be deoxymannose. Doses for patients (usually 5 to 10 mCi, or ~0.25 mg) were sterile and pyrogen free.

Animal Preparations

Eight dogs and 2 rhesus monkeys were lightly anesthetized with sodium pentobarbital (25 mg per kilogram of body weight), and catheters were placed in the femoral artery for

blood sampling and in two leg veins for blood sampling and injection of FDG. Supplemental doses of sodium pentobarbital were given as needed.

Human Studies

Under local anesthesia, an arterial catheter was placed in a brachial artery for blood sampling in 12 volunteers. A 23-gauge needle was placed in an arm or hand vein of each arm for injection of FDG and blood sampling. In some of the studies, venous blood was drawn from the vein of a hand heated to 44°C in a hot-water glove box to arterialize venous blood for comparison to arterial sampling. In the remaining subjects, FDG was injected intravenously and blood was sampled only from a vein of the heated hand of the opposite arm. Studies were performed under informed consent, and all procedures accorded with the UCLA School of Medicine Human Use Committee.

Blood Sampling, Analysis, and Counting

Concurrent with a 30-second to 1-minute intravenous injection of FDG, 2 ml samples of arterial or venous blood, or both, were taken every 10 to 15 seconds for the first 1½ to 2 minutes, with sample intervals progressively lengthened. Samples were immediately put on ice and subsequently centrifuged to separate plasma for the determination of plasma glucose and FDG concentrations. Before injection of FDG and throughout the study, blood samples were also taken for measurement of pH, blood gases, and hematocrit. Plasma glucose concentrations were determined by standard enzymatic techniques in duplicate. Blood gases (CO_2 and O_2) and pH were determined by standard clinical laboratory techniques.

The precision of the plasma glucose analysis was determined by analyses of three different sets of 30 samples run in either duplicate or triplicate. The average standard deviation from the mean (99.6 mg/dl) was ± 2.1. The plasma concentration of FDG was determined by counting a known volume determined with analytical pipettes (± 0.5% accuracy as determined by comparison to sample weights) or by weighing.

Imaging

All PCT images were obtained with the ECAT, a positron imaging system developed by Phelps and Hoffman [36, 40, 41] and capable of providing quantitative tomographic and two-dimensional images. The video display system, in conjunction with the joy stick and utility software of the system, was used for data analysis.

Images from subjects were obtained at multiple levels when concentrations of radioactivity in whole brain were required. Images from a single slice were taken as a function of time for determination of the kinetic rate constants and to measure the stability and precision of the CMRGlc calculation.

The ECAT was calibrated by imaging a uniform cylinder of positron activity (F-18) from which a known volume of radioactivity was taken for counting in a NaI(Tl) well counter under the same conditions as the blood samples. This provides a calibration factor between the ECAT and the well counter for determination of absolute metabolic rates. This calibration factor, f, is equal to:

$$f = \frac{(c/sec)(\mu Ci/cm^2)^{-1} \text{ (in ECAT image)}}{(c/sec)(\mu Ci/ml)^{-1} \text{ (in well counter)}} \quad (1)$$

The medium-resolution mode of the ECAT was used in these studies, with a measured resolution of 1.3 cm full-width half-maximum (FWHM) of a line source in the plane and 1.9 cm FWHM in the axial direction [40]. The ECAT has been well characterized in terms of resolution, efficiency, scatter and random coincidence fractions, count rate linearity, and recovery of tissue concentrations as a function of object size [22, 40].

Metabolic Model

Abbreviations and symbols used are shown on page 374. The model utilized in this work is an extension of the (C-14) DG model developed by Sokoloff et al [53] for autoradiography.

This model assumes three compartments, viz, a blood compartment, a compartment for metabolic precursors (glucose, FDG) in tissue, and a compartment for metabolic products (glucose-6-PO_4 and FDG-6-PO_4) in tissue, as shown in Figure 1. These three compartments are referred to as compartments 1, 2, and 3, respectively. The boundary between compartments 1 and 2 is the capillary membrane. That between compartments 2 and 3 is not a physical barrier but a phosphorylation reaction catalyzed by hexokinase. The rate of transfer of FDG across cell membranes has been shown not to be rate limiting [1, 32] as compared to the rate of its phosphorylation within cells by hexokinase. Thus the cell membranes can be disregarded (or capillary and cell membranes can be thought of as one) in the form of the operational model equation of Sokoloff et al [53]. In this model, if DG-6-PO_4 is trapped in compartment 3, its concentration is directly related to CMRGlc. The form of the equation used by Sokoloff et al to calculate CMRGlc is given by:

$$\text{CMRGlc} = \frac{C_P\left[C_i^*(T) - k_1^* e^{-(k_2^*+k_3^*)T}\int_0^T C_P^*(t)e^{(k_2^*+k_3^*)t}dt\right]}{LC\left[\int_0^T C_P^*(t)dt - e^{-(k_2^*+k_3^*)T}\int_0^T C_P^*(t)e^{(k_2^*+k_3^*)t}dt\right]} \quad (2)$$

where the mean capillary plasma concentrations of glucose, C_P, and FDG, $C_P^*(t)$, have been approximated by arterial values by both Sokoloff et al [53] and Reivich et al [48, 49]. LC is given by:

$$LC = \frac{\lambda V_m^* K_m}{\phi V_m K_m^*} \quad (3)$$

Sokoloff's model assumes that once FDG is phosphorylated by hexokinase to FDG-6-PO_4, it is not cleared to any great degree during the time of the study because the activity of phosphatase, which hydrolyzes FDG-6-PO_4 to

CMRGlc	Cerebral metabolic rate for glucose
LCMRGlc	Local CMRGlc
DG	2-Deoxy-D-glucose
FDG	(F-18)2-fluoro-2-deoxy-D-glucose
*	Superscript asterisk denotes symbols which apply to FDG; symbols without asterisk apply to glucose
$\otimes$	Denotes operation of convolution
k_1^*, k_2^*	First-order rate constants for FDG forward and reverse capillary membrane transport, respectively (Fig 1)
k_3^*, k_4^*	First-order rate constants for phosphorylation of FDG and dephosphorylation of FDG-6-PO_4, respectively (Fig 1)
LC	Lumped constant: ratio of arteriovenous extraction fraction of FDG to that of glucose under steady-state conditions and when k_4^* is small
λ	Ratio of distribution volume of FDG to that of glucose: $\lambda = [k_1^*/(k_2^* + k_3^*)]/[k_1/(k_2 + k_3)]$ when k_4^* is small
V_m	Maximum velocity of phosphorylation of glucose (V_m^* is for FDG)
K_m	Michaelis-Menton constant for phosphorylation of glucose (K_m^* is for FDG)
ϕ	Ratio of the differences between the rates of phosphorylation and dephosphorylation of glucose to its rate of phosphorylation
$C_i^*(t)$, $C_i^*(T)$	Cerebral tissue concentration of FDG plus FDG-6-PO_4 in region i as a function of time (t) or at a single time (T)
C_P	Capillary plasma glucose concentration (steady state); approximated by average value from peripheral artery or vein
$C_P^*(t)$	Capillary plasma FDG concentration as a function of time; approximated by values from peripheral artery or vein
C_E, C_M	Steady-state tissue concentration of glucose and glucose-6-PO_4, respectively
$C_E^*(t)$, $C_M^*(t)$	Tissue concentration of FDG and FDG-6-PO_4, respectively, as a function of time (t)
α_1, α_2	Rate constants for the model response to an impulse change in FDG capillary plasma concentration

FDG + PO_4, is low in brain. Our studies indicate that loss of FDG-6-PO_4, although slow, is sufficient to cause significant errors, depending upon how long after injection CMRGlc is measured. Thus we have derived an extension of Sokoloff's model which allows for hydrolysis of FDG-6-PO_4 to FDG [23]. The rate of FDG formed in this manner (k_4^*) then competes between the rate of clearance to blood (k_2^*) and the rate of rephosphorylation (k_3^*) to FDG-6-PO_4 (see Fig 1).

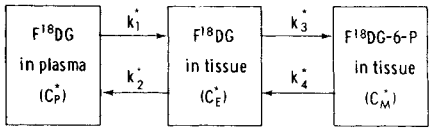

Fig 1. The three-compartment model for measurement of cerebral metabolic rate for glucose with (F-18)2-fluoro-2-deoxy-D-glucose (FDG). The Sokoloff et al [53] model employed (C-14)2-deoxy-D-glucose and considered only k_1^*, k_2^*, and k_3^*. Our model, which is an extension of Sokoloff's, includes k_4^*-mediated hydrolysis of FDG-6-PO_4 → FDG + PO_4 (Eq 23).

Derivation of Operational Equation for CMRGlc Model

The rates of change of $C_E^*(t)$ and $C_M^*(t)$ in the compartmental model of Figure 1 can be expressed as:

$$\frac{d}{dt}C_E^*(t) = k_1^*C_P^*(t) - (k_2^* + k_3^*)\,C_E^*(t) + k_4^*C_M^*(t) \quad (4)$$

$$\frac{d}{dt}C_M^*(t) = k_3^*C_E^*(t) - k_4^*C_M^*(t) \quad (5)$$

From these two simultaneous linear differential equations, $C_E^*(t)$ and $C_M^*(t)$ can be solved in terms of $C_P^*(t)$:

$$C_E^*(t) = \frac{k_1^*}{\alpha_2 - \alpha_1}[(k_4^* - \alpha_1)e^{-\alpha_1 t} + (\alpha_2 - k_4^*)e^{-\alpha_2 t}] \otimes C_P^*(t) \quad (6)$$

$$C_M^*(t) = \frac{k_1^*k_3^*}{\alpha_2 - \alpha_1}(e^{-\alpha_1 t} - e^{-\alpha_2 t}) \otimes C_P^*(t) \quad (7)$$

where

$$\alpha_1 = [k_2^* + k_3^* + k_4^* - \sqrt{(k_2^* + k_3^* + k_4^*)^2 - 4k_2^*k_4^*}]/2 \quad (8)$$

$$\alpha_2 = [k_2^* + k_3^* + k_4^* + \sqrt{(k_2^* + k_3^* + k_4^*)^2 - 4k_2^*k_4^*}]/2 \quad (9)$$

and $\otimes$ denotes the operation of convolution, that is:

$$a(t) \otimes b(t) = \int_0^t a(\tau)b(t - \tau)d\tau \quad (10)$$

The total amount of tracer in tissue, $C_i^*(t)$, is equal to the sum of $C_E^*(t)$ and $C_M^*(t)$. The amount of tracer attributable to the vascular compartment is negligible because the vascular space in tissue is small compared with the extravascular space. Thus,

$$C_i^*(t) = C_E^*(t) + C_M^*(t) \quad (11)$$

Substituting $C_E^*(t)$ and $C_M^*(t)$ from Eqs. 6 and 7, Eq. 11 becomes:

$$C_i^*(t) = \frac{k_1^*}{\alpha_2 - \alpha_1}[(k_3^* + k_4^* - \alpha_1)e^{-\alpha_1 t} + (\alpha_2 - k_3^* - k_4^*)e^{-\alpha_2 t}] \otimes C_P^*(t) \quad (12)$$

In a steady state, LCMRGlc is equal to the net phosphorylation rate of glucose; that is:

$$\text{LCMRGlc} = k_3C_E - k_4C_M = \phi\, k_3C_E \quad (13)$$

where $\phi \equiv 1 - k_4C_M/k_3C_E$ is the fraction of glucose that is metabolized after it is phosphorylated. Also, there is no net accumulation or depletion of glucose in a steady state. Thus,

$$k_1C_P + k_4C_M = k_2C_E + k_3C_E$$

or

$$C_E = \frac{k_1}{k_2 + \phi k_3} C_P \tag{14}$$

and

$$LCMRGlc = \frac{k_1k_3\phi}{k_2 + \phi k_3} C_P \tag{15}$$

By multiplying both the numerator and the denominator of Eq. 15 by $k_1^*k_3^*/(k_2^* + k_3^*)$, LCMRGlc can be expressed as:

$$LCMRGlc = \left(\frac{k_1^*k_3^*}{k_2^* + k_3^*}\right)\left(\frac{k_3}{k_3^*}\right)\left(\frac{k_1/(k_2 + k_3\phi)}{k_1^*/(k_2^* + k_3^*)}\right)C_P\phi$$

$$= \left(\frac{k_1^*k_3^*}{k_2^* + k_3^*}\right)\left(\frac{\phi}{\lambda f}\right) C_P \tag{16}$$

where $f = k_3^*/k_3$ and $\lambda = [k_1^*/(k_2^* + k_3^*)]\,[k_1/(k_2 + k_3\phi)]^{-1}$.

Since FDG and glucose are competitive substrates for hexokinase in the phosphorylation process, their rates follow the Michaelis-Menton relationship; that is:

$$k_3^* = \frac{V_m^*/K_m^*}{1 + C_E/K_m + C_E^*/K_m^*} \tag{17}$$

$$k_3 = \frac{V_m/K_m}{1 + C_E/K_m + C_E^*/K_m^*} \tag{18}$$

where V_m and V_m^* are maximum velocities and K_m, K_m^* are apparent Michaelis-Menton constants for glucose and FDG. Thus,

$$f = V_m^*K_m/V_mK_m^* \tag{19}$$

and

$$\frac{\lambda f}{\phi} = \frac{\lambda V_m^*K_m}{\phi V_mK_m^*} \tag{20}$$

This factor has the same form as the lumped constant in Sokoloff's model [53] and is similarly denoted as LC. Then:

$$LCMRGlc = \frac{C_P}{LC}\left(\frac{k_1^*k_3^*}{k_2^* + k_3^*}\right) \tag{21}$$

By multiplying both the numerator and the denominator with $C_M^*(T)$, LCMRGlc can be expressed as:

$$LCMRGlc = \frac{C_P}{LC}\left(\frac{k_1^*k_3^*}{k_2^* + k_3^*}\right)\left(\frac{C_M^*(T)}{C_M^*(T)}\right)$$

$$= \frac{C_P}{LC}\left(\frac{k_1^*k_3^*}{k_2^* + k_3^*}\right)\left(\frac{C_I^*(T) - C_E^*(T)}{C_M^*(T)}\right) \tag{22}$$

Substituting C_E^* and C_M^* from Eqs. 6 and 7, Eq. 22 becomes:

$$LCMRGlc = \frac{C_P\left(C_I^*(T) - \frac{k_1^*}{\alpha_2 - \alpha_1}[(k_4^* - \alpha_1)e^{-\alpha_1 t} + (\alpha_2 - k_4^*)e^{-\alpha_2 t}] \otimes C_P^*(t)\right)}{LC\left(\frac{k_2^* + k_3^*}{\alpha_2 - \alpha_1}\right)\left(e^{-\alpha_1 t} - e^{-\alpha_2 t}\right) \otimes C_P^*(t)} \tag{23}$$

Thus, LCMRGlc can be calculated according to Eq. 23 from the measured quantities of C_P, $C_P^*(t)$, and $C_I^*(T)$. The symbol t is used in Eq. 23 to denote the requirement of the full time course of $C_P^*(t)$ up to time T, as compared to the value of $C_I^*(T)$ at a single time T.

The assumptions of Eq. 2 (which also apply to Eq. 23 with the exception that $k_4^* \neq 0$) have been extensively discussed by Sokoloff et al [53]. Some pertinent assumptions and issues concerning this model are discussed in the following sections.

Determination of Rate Constants and Lumped Constant

The rate constants, k_1^* to k_4^*, can be determined with Eq. 12 if the rate of change of total tissue F-18, plasma FDG, and plasma glucose concentrations are known as a function of time. The tissue measurements were performed by using the ECAT to image the same region of the brain repeatedly over time periods of 3 to as much as 14 hours after injection. Early images were taken at 30- to 300-second intervals, with longer intervals as the study progressed. This resulted in time concentration curves with 20 to 50 data points. The images at 2 to 14 hours were required to determine the small k_4^* term accurately. Since the k*s correspond to half-times of minutes to hours (Table 1), the sampling times used in this work produced no significant loss in accuracy. These data, together with the concentration of FDG in arterial or "hot vein" plasma, were used with Eq. 12 to calculate the values of the k*s by a least-squares curve-fitting method. Values for gray and white matter were calculated by using the region-of-interest programs of the ECAT to isolate individual regions (about 1 to 3 cm^2) of gray and white matter. The levels studied ranged from the basal ganglia to 9 cm above the orbital meatus.

The LC was estimated for human subjects by initially calculating (Eq. 23) the CMRGlc for gray and white structures in the different cross-sections with LC set equal to unity. These values of CMRGlc were weighted to yield a whole-brain CMRGlc on the assumption that brain is 50% gray and 50% white matter [25]. The ratio of these values to the average CMRGlc (weighted by reported error estimates) of 5.38 ± 0.77 (1 SD) mg per minute per 100 gm of tissue reported for humans [8, 15, 33, 51, 55] is equal to the LC for FDG.

Table 1. Rate Constants for DG and FDG in Brain

Constant	Deoxyglucose				Fluorodeoxyglucose in Human Brain[c] (this work)	
	In Rat Brain[a]		In Monkey Brain[b]			
	Gray Matter	White Matter	Gray Matter	White Matter	Gray Matter	White Matter
k_1^* (min^{-1})	0.189 (±0.012)	0.079 (±0.008)	...	...	0.102 (±0.029)	0.054 (±0.015)
k_2^* (min^{-1})	0.245 (±0.040)	0.133 (±0.046)	...	...	0.130 (±0.066)	0.109 (±0.044)
k_3^* (min^{-1})	0.052 (±0.010)	0.020 (±0.020)	...	...	0.062 (±0.019)	0.045 (±0.019)
k_4^* (min^{-1})	...	...	...	...	0.0068 (±0.0014)	0.0058 (±0.0017)
$k_2^* + k_3^*$ (min^{-1})	0.297	0.153	0.347	0.144	0.192 (±0.079)	0.154 (±0.058)
LC	0.483 (±0.022)		0.344 (±0.036)		0.420 (±0.059)	

[a]Sokoloff et al [53]. Values for errors are *standard error of the mean* for different animals and different gray and white matter structures of the brain.
[b]Kennedy et al [26]. Error is *standard error of the mean.*
[c]Values for errors are *1 standard deviation* from the mean of multiple measurements of gray and white matter.

Compartmental Concentration of FDG and FDG-6-PO_4

Compartmental concentration of FDG and FDG-6-PO_4 as a function of time was determined from measured values of tissue F-18 concentration, arterial (or hot vein) plasma FDG, and Eqs. 6 and 7 with our measured values of k*s. This approach was used to isolate and inspect the time course of free FDG and FDG-6-PO_4 concentrations in cerebral tissue for both gray and white matter.

In addition, the tissue plasma FDG concentration was determined by measuring the cerebral blood volume (CBV) with ^{11}CO-labeled red blood cells (RBC) and the ECAT by the method developed by Phelps et al [38] for x-ray fluorescence and applied to ECT by Kuhl et al [31]. The fraction (f_P) of total tissue F-18 concentration in the cerebral plasma compartment was then calculated by:

$$f_P = \frac{C_P^*(T)(CBV)(1 - 0.85H)}{C_I^*(T)} \quad (24)$$

where values are determined at selected points in time T, H is the large vessel hematocrit, and 0.85 is the correction for the difference between large vessel and cerebral hematocrit [38]. In these studies the region of the brain defined by the FDG images was used for measurement of CBV (i.e., this approach excluded CBV of extracerebral vessels and some superficial vessels of the brain and corresponded directly to the CBV of the tissue for which CMRGlc was measured). The technique was applied to 3 persons with an average cross-sectional CBV of 0.031 ± 0.0062 ml per gram of tissue. This is about 0.5 to 0.75 of the average values reported for CBV that typically includes superficial cerebral vessels [16–18, 27, 31, 37, 38, 52]. The ratio of plasma to red blood cell FDG concentrations was also measured to allow calculation of either tissue blood or plasma concentrations.

RBC/Plasma Concentration Gradient

Blood samples from 14 individuals were taken as a function of time, and red blood cell and plasma F-18 concentrations were measured.

Replacement of Arterial Blood Sampling with Venous Blood Sampling

Arterial plasma values of DG and glucose were used by Sokoloff et al [53] and Reivich et al [48, 49] as an estimate of the mean capillary plasma values. To reduce trauma to the subject, we investigated the use of venous sampling from a resting arm or hand. Since the area under the FDG plasma concentration ($C_P^*(t)$) curve is proportional to the input function of the model (Eqs. 2, 23), the validity of this approach was evaluated by measuring the ratio of these areas for peripheral vein ($C_P^*(t)_V$) to artery ($C_P^*(t)_A$) plasma concentration, as given by:

$$\int_0^T C_P^*(t)_V dt \Big/ \int_0^T C_P^*(t)_A dt \quad (25)$$

The plasma glucose concentration (C_P) also appears in the model, so the ratio of venous to arterial plasma glucose concentration was determined:

$$(C_P)_V/(C_P)_A \quad (26)$$

If the ratio in Eq. 25 or, better, the ratio of Eqs. 25 to 26 is one (the values for FDG and glucose appear in the denominator and numerator of Eq. 23 and tend to partially

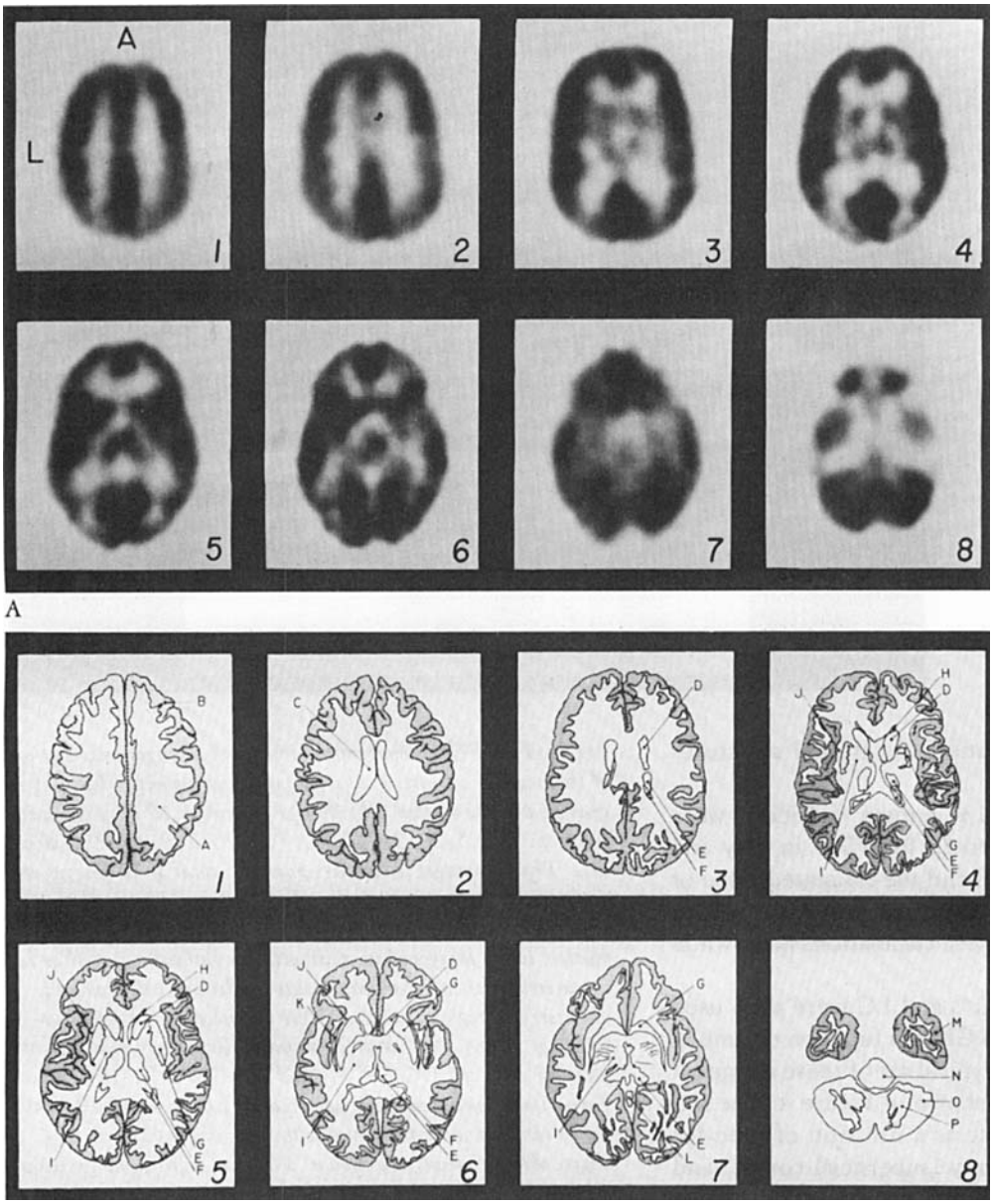

B

Fig 2. (A) CMRGlc images for selected cross-sections ranging from 8 cm above to 1 cm below the orbital meatus in a human volunteer. Progression is from left to right and top to bottom; L is left side and A is anterior. Increasing tissue activity concentration is shown as darker shades of gray. Note the clear delineation of superficial cortex, subcortical white matter, and internal gray nuclei. Images are at 1.3 cm resolution. (B) Sketches of anatomical structures for comparison to CMRGlc images. Figure numbers in A and B are for approximate correspondence of levels. Figures were traced from actual brain slices, and only major structures are shown for clarity. (A = *subcortical white matter;* B = *superficial cortex;* C = *lateral ventricle;* D = *caudate nucleus;* E = *thalamic nuclei;* F = *atrium of lateral ventricle;* G = *putamen and globus pallidus;* H = *anterior horn of lateral ventricle;* I = *internal capsule;* J = *external capsule;* K = *claustrum;* L = *vermis;* M = *temporal lobe;* N = *pons;* O = *cerebellar hemisphere;* P = *cerebellar white matter.)*

cancel), then the substitution of venous for arterial sampling is valid. These ratios were determined in 8 dogs, 2 monkeys, and 6 human subjects.

As a further improvement, we determined these ratios in 4 human subjects whose venous blood was drawn from a hand heated to about 44°C in a specially designed hot water box. The heating of the hand "arterializes" the venous blood by large increases in blood flow without a concomitant rise in metabolism [13, 56]. This flow increase is a cooling mechanism (i.e., hyperemia or luxury perfusion).

Results

Kinetic Constants and CMRGlc

Figure 2 is a set of tomographic images of CMRGlc in a normal volunteer from levels 8 cm above to 1 cm below the orbital meatus. The figure illustrates the

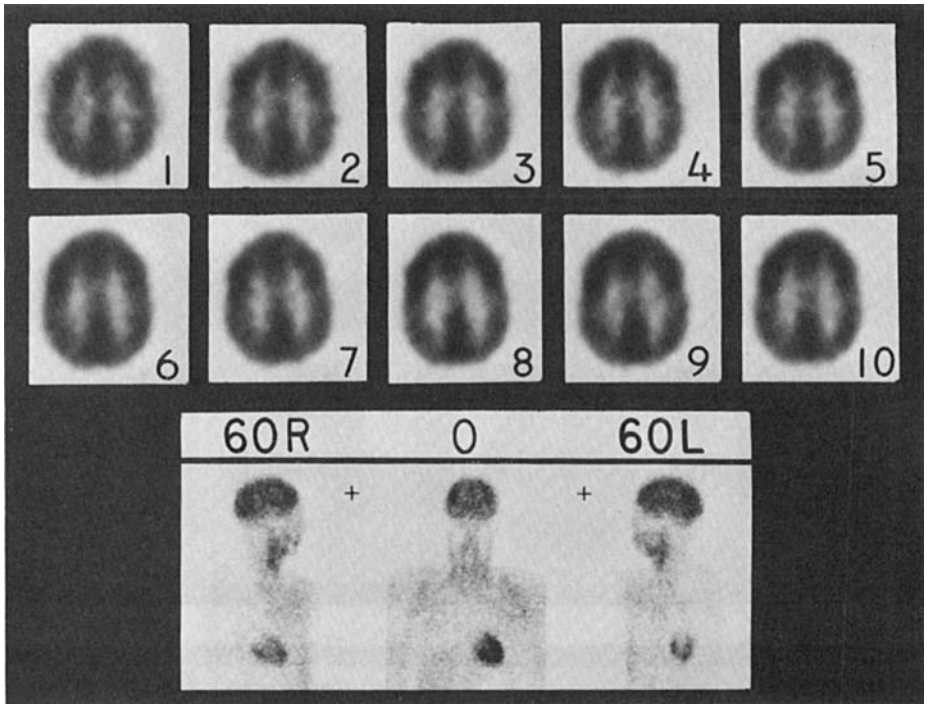

Fig 3. (Top) FDG tomographic images of a single cross-section of the head as a function of time for measurement of k_1^* to k_4^* in gray and white matter. The images 1 through 10 have midscan times of 2.5, 7.5, 20, 30, 40, 60, 70, 120, 240, and 300 minutes. The 10 images shown are part of a total of 40 images recorded. Level is 9 cm above the orbital meatus. Images show superficial cortex, intercerebral cortex, and subcortical white matter. Early images show radioactivity in brain as well as in extracerebral tissue. As steady-state condition is approached, only cerebral regions are seen. Note consistency and reproducibility of images after about 20 minutes. Resolution was medium, and 4.5 mCi of FDG was injected intravenously. (Bottom) Two-dimensional images of upper torso. The three simultaneous views recorded with the tomograph (zero degrees and ± 60-degree oblique views) are shown. The plus signs show position selected for tomography.

image quality and delineation of cerebral structures achieved in this study.

Serial images from 13 human subjects were analyzed to calculate k_1^* to k_4^* for FDG in gray and white matter. These values and the estimated value of LC are given in Table 1. A typical set of images (at selected times) used for these calculations is shown in Figure 3.

The average values of k*s and LC were then used to calculate the local CMRGlc as a function of time in 11 normal volunteers. A typical set of these images at selected time intervals is shown in Figure 4. The numerical values of CMRGlc as a function of time for about 2 cm^2 regions of gray (superficial cortex) and subcortical white matter from 4 volunteers are shown in Figure 5. The precision of the local CMRGlc determinations was better than ±5.5% over a 3- to 4-hour period and ±4% during the period between 40 and 80 minutes after injection, during which we typically measured CMRGlc in patients.

Compartmental Concentrations of FDG and FDG-6-PO_4

Equations 6 and 7, our values of k*s, the measured F-18 tissue concentration, and plasma FDG concentrations were used to calculate the tissue FDG and FDG-6-PO_4 concentrations as a function of time. A typical example for gray and white matter is shown in Figure 6. Table 2 gives the mean values for 10 human subjects as compared with published values in rats and mice.

The measured value (Eq. 24) of the fraction (f_P) of total tissue F-18 concentration which is FDG in tissue plasma is shown in Figure 7. These values are for whole brain, excluding plasma activity in superficial vessels (see Methods). These values can be converted to whole blood values (f_B) by:

$$f_B = \frac{f_P\,[RBC]/[plasma]\,(0.85H)}{(1 - 0.85H)} + f_P \qquad (27)$$

where [RBC]/[plasma] is the ratio of red blood cell to plasma F-18 concentration (see Fig 8), H is hematocrit (average value of H in this work was 0.39 ± 0.01), and 0.85 is the cerebral hematocrit correction [38]. For example, at 40 minutes, $f_B = 1.43\ f_P$.

The average values of f_P or f_B for gray and white matter can be calculated from the average gray and white matter CBV values of 0.042 ± 0.005 and

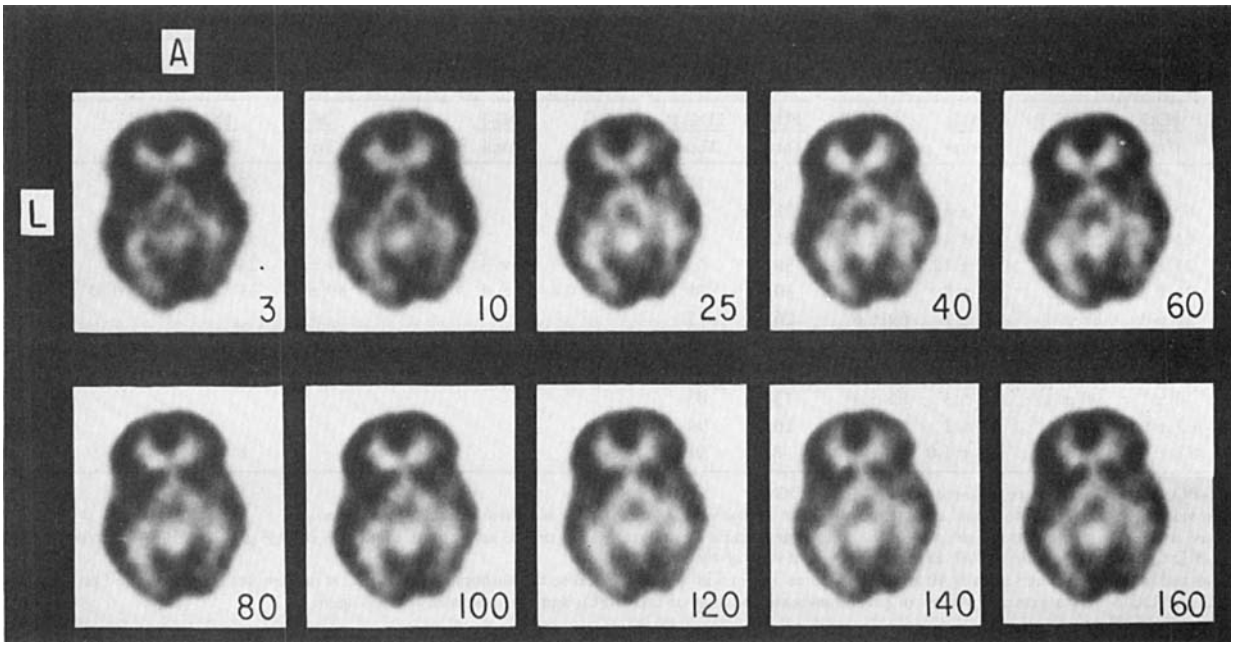

Fig 4. A single cross-section of the head as a function of time for determination of stability and precision of measurement of CMRGlc with FDG. Mid-times of scans are shown below images. The images shown were selected from a total of 30. Level is 3.5 cm above the orbital meatus (level of basal ganglia). L is left and A is anterior. Note clear delineation of the superficial cortex, internal capsule, caudate nuclei (left and right), thalamus, and visual cortex. Note reproducibility of images after about 10 minutes. Resolution was medium, and 6 mCi of FDG was injected.

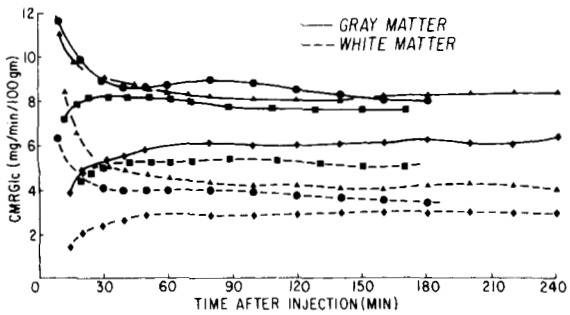

*Fig 5. CMRGlc calculated from Eq. 23 as a function of time for gray and white matter regions (each region is about 2 cm^2) of brain from 4 volunteers, illustrating the typical variability we have observed. Note that at early times (<30 min) some variability is seen. This is because steady state has not been reached, and the calculated value of CMRGlc is heavily dependent upon the exact values of k*s (see Discussion). After 30 minutes this dependence is decreased and the calculation is much more stable and reproducible. Some variations in actual cerebral metabolism may also be occurring during the study. Values of local CMRGlc were found to be in good agreement with values in rhesus monkey from autoradiographic studies with DG [26]. Because of variability at early times, measurements of CMRGlc in patients are started 30 to 40 minutes after the injection.*

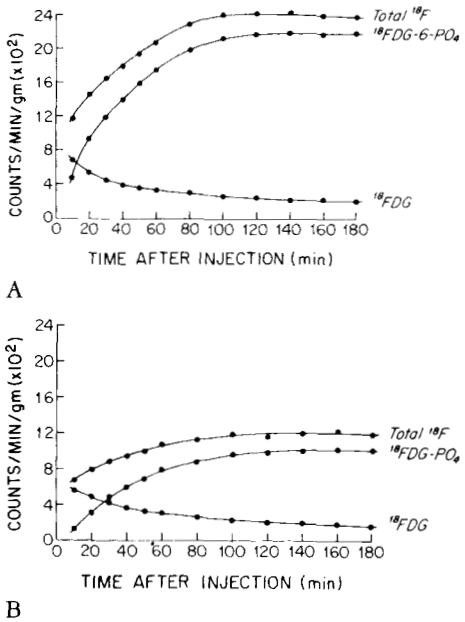

Fig 6. Typical temporal distributions of F-18 activity in gray (A) and white (B) matter between free FDG and FDG-6-PO_4 in a human subject. Compartmental concentrations were calculated from Eqs. 6 and 7 as described in Methods. Note that total measured tissue F-18 and calculated FDG-6-PO_4 increase steadily over the first 80 to 100 minutes due to continual trapping or sequestering of FDG-6-PO_4. Average distribution values from human studies are shown in Table 2.

Table 2. Percentage of Tissue Activity in the Free Form and Phosphorylated Deoxyglucose and Fluorodeoxyglucose[a]

Time (min)	Human Gray Matter[b] FDG Total	Human Gray Matter[b] FDG-P Total	Human White Matter[b] FDG Total	Human White Matter[b] FDG-P Total	Human Whole Brain[c] FDG Total	Human Whole Brain[c] FDG-P Total	Rat Gray Matter[d] DG Total	Rat Gray Matter[d] DG-P Total	Rat White Matter[d] DG Total	Rat White Matter[d] DG-P Total	Rat Whole Brain[e] DG Total	Rat Whole Brain[e] DG-P Total	Mouse Whole Brain[f] FDG-P Total
5	75 ± 4	24 ± 4	82 ± 7	18 ± 8	79	21					67	33	95
10	67 ± 13	34 ± 14	77 ± 8	21 ± 9	72	28					29	71	
20	41 ± 7	59 ± 7	60 ± 13	39 ± 12	51	49					33	67	
30	29 ± 5	71 ± 6	46 ± 12	54 ± 12	38	63	15.0 ± 0.5	85 ± 3	36 ± 2	64 ± 4	26	74	89
40	24 ± 4	77 ± 5	36 ± 8	64 ± 18	30	71	9.0 ± 0.4	91 ± 4	20 ± 1	80 ± 4	13	86 (87)	
50	20 ± 3	81 ± 4	31 ± 5	69 ± 6	26	75							
60	16 ± 2	84 ± 2	25 ± 3	76 ± 3	21	80	7.5 ± 0.3	93 ± 4	14.0 ± 0.3	86 ± 2			93
80	13 ± 1	87 ± 2	23 ± 3	78 ± 4	18	83							
120	10 ± 1	90 ± 1	16 ± 3	85 ± 3	13	88							92
180	8.2 ± 0.8	92 ± 1	12 ± 2	88 ± 2	10	90							
240	6.8 ± 0.6	93 ± 1	9.1 ± 1.0	91 ± 1	8	92					8	79 (92)	

[a]FDG-6-PO_4 and DG-6-PO_4 are denoted as FDG-P and DG-P.
[b]Human values are from this work and are mean values for 10 subjects; the errors are *standard deviation from the mean.*
[c]Estimated whole brain values are derived from the human gray and white matter values on the assumption that brain is 50% gray and 50% white matter [25].
[d]Sokoloff L: unpublished results, 1979. Errors are *standard error of the mean.*
[e]Hawkins and Miller [19]. The values at 40 and 240 minutes do not add to 100% because the authors reported that at these times an unidentified product other than DG and DG-6-PO_4 is present. Values in parentheses are the sum of DG-6-PO_4 and the unknown labeled agent.
[f]Gallagher et al [12].

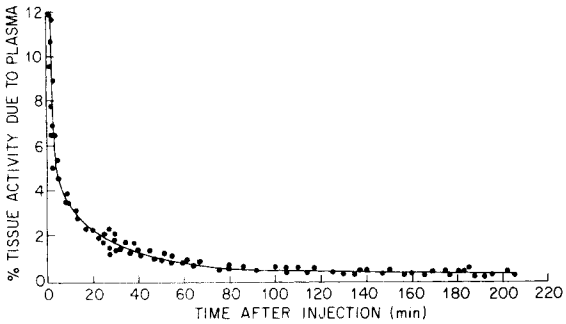

Fig 7. Percentage of average cerebral tissue activity in plasma of the vascular compartment (Eq. 24) as a function of time in human subjects. Percentage in the total blood compartment and values for plasma and blood in gray and white matter can be calculated from data in this figure, Figure 8, and Eqs. 27 and 28. Tissue plasma and total blood FDG in cerebral tissue rapidly decrease to a small fraction of total tissue activity.

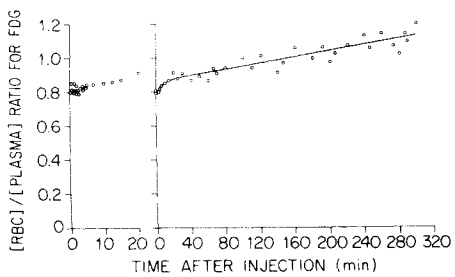

Fig 8. Concentration ratio of F-18 in red blood cells to that of plasma from 10 human subjects. The [RBC]/[plasma] ratio slowly increases, apparently due to sequestering of FDG-6-PO_4 in RBCs. Initial values are shown in the expanded scale at left.

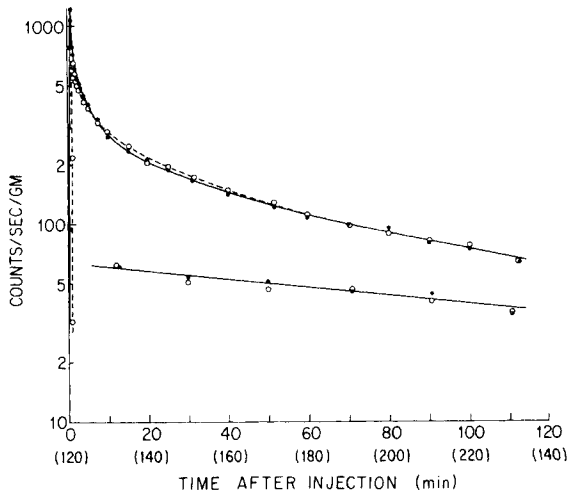

Fig 9. Normal resting arterial (solid curve) *and venous* (dotted curve) *FDG plasma curves across a resting arm. Initially, unidirectional transport of FDG produces a large (A-V)/A value of 58% even though the glucose value is only 4%. Then as arterial FDG concentration decreases and reverse transport of FDG takes place, the venous values become larger than arterial ones. As steady state is reached, the (A-V)/A values for FDG and glucose run in parallel and differ due to LC for FDG in the arm. Times in parentheses apply to lower curve.*

0.021 ± 0.006 ml per gram measured in this work. The average F-18 concentration in gray matter was found to be 2.1 ± 0.5 times white matter. This, together with the average whole-brain CBV of 0.032 ± 0.0062, can be used to calculate f_P(gray) by:

$$f_P(\text{gray}) = f_P\left(\frac{0.042}{0.032}\right)\left(\frac{1.55}{2.1}\right) = 0.97\, f_P \qquad (28)$$

where 0.042/0.032 and 1.55/2.1 are the conversion factors from average brain values to gray matter val-

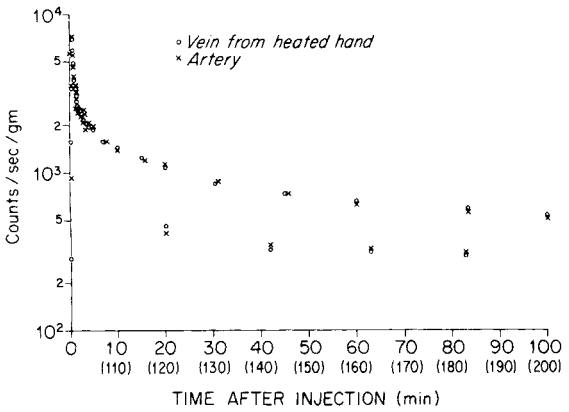

Fig 10. Arterial (crosses) *and venous* (circles) *FDG plasma clearance in which venous blood samples were taken from a hand heated to 44°C in a specially designed water glove box. Heating was used to "arterialize" the hand vein, as demonstrated by superimposition of the data (see Table 4).*

ues of CBV and tissue F-18 concentration. A similar result can be used to calculate f_P(white), f_B(gray), and f_B(white).

The ratio of F-18 concentration in RBC to that in plasma from 10 human subjects is plotted in Figure 8 as a function of time. No significant difference was found in this ratio between arterial and venous blood.

Arterial versus Venous Blood Sampling

Examples of arterial (A) and venous (V) FDG plasma curves across the hand or arm of human subjects are shown in Figures 9 and 10. Figure 9 shows the A and V FDG plasma curves of a typical resting arm, and Figure 10 shows the A and V FDG plasma curves when blood was drawn from the vein of a hand heated to 44°C to arterialize the venous blood.

Table 3 shows the ratio of the venous to arterial FDG plasma input functions (Eq. 25) along with the

Table 3. Venous to Arterial FDG Plasma Input Function Ratio (V/A(FDG)), Average Ratios of Venous to Arterial Plasma Glucose (V/A(Glc)), and Ratio of These Two Factors from a Resting Leg of a Dog and Monkey and a Human Arm[a]

Time after Injection (min)	Dog and Monkey			Human		
	V/A(FDG)	V/A(Glc)	V/A(FDG) / V/A(Glc)	V/A(FDG)	V/A(Glc)	V/A(FDG) / V/A(Glc)
5	0.86 (0.15)	0.93 (0.04)	0.94 (0.15)	0.89 (0.20)	0.97 (0.10)	0.92 (0.07)
10	0.91 (0.12)	0.95 (0.03)	0.95 (0.13)	0.91 (0.15)	0.95 (0.07)	0.93 (0.09)
20	0.94 (0.10)	0.95 (0.04)	0.99 (0.12)	0.94 (0.13)	0.96 (0.07)	0.98 (0.08)
30	0.96 (0.06)	0.97 (0.03)	0.99 (0.07)	0.93 (0.11)	0.96 (0.08)	0.97 (0.06)
40	0.98 (0.07)	0.96 (0.05)	1.02 (0.07)	0.89 (0.08)	0.92 (0.10)	1.01 (0.06)
60	0.98 (0.06)	0.99 (0.04)	0.99 (0.06)	0.91 (0.09)	0.90 (0.08)	0.99 (0.04)
90	0.99 (0.06)	0.98 (0.04)	1.01 (0.06)	0.90 (0.08)	0.89 (0.06)	1.01 (0.03)
120	0.99 (0.05)	0.97 (0.03)	1.02 (0.05)	0.91 (0.08)	0.89 (0.06)	1.01 (0.04)
180	1.00 (0.05)	0.98 (0.03)	1.02 (0.04)	0.92 (0.09)	0.88 (0.08)	1.04 (0.08)
220	0.99 (0.05)	0.97 (0.03)	1.03 (0.05)	...	...	...

[a]Data from 8 dogs, 2 monkeys, and 6 human subjects. V/A(FDG) is Eq. 25 for plasma FDG; V/A(Glc) is Eq. 26 for plasma glucose. The time of integration or averaging is from 0 to time T after injection (column 1). Values in parentheses are 1 standard deviation (SD). The average arterial glucose value was 88 ± 8 (±SD) for animals and 98 ± 5 (±SD) for humans. The average extraction fraction for glucose was 0.036 ± 0.010 (±SD) for animals and 0.075 ± 0.021 (±SD) for humans.

Table 4. Comparison of Blood Sampling from Brachial Artery, Normal Hand Vein, and Hand Vein Heated to 44°C[a]

Time (min)	Heated V / A (FDG)[b]	Determination	Normal Vein	Heated Vein	Artery
5	0.98 ± 0.01	pH	7.38 ± 0.01	7.43 ± 0.02	7.43 ± 0.02
10	0.99 ± 0.02	P_{CO_2} (mm Hg)	39.3 ± 2.1	35.0 ± 1.8	35.0 ± 1.7
30	0.99 ± 0.03	P_{O_2} (mm Hg)	39.1 ± 4.2	78.0 ± 3.4	85.1 ± 3.6
60	1.00 ± 0.02	Glucose (mg/100 ml)	81.9 ± 4.8	87.0 ± 4.1	86.7 ± 5.2
90	1.01 ± 0.02				
180	1.02 ± 0.03				

[a]Values are mean with 1 standard deviation. Data are from 4 human subjects.
[b]From Eq. 25.

average venous to arterial plasma glucose concentration (Eq. 26) as a function of time. Values are given for the resting arm (humans) or leg (dogs and monkeys). Values from artery and hot vein are given in Table 4.

Discussion

Kinetic Rate Constants

Since kinetic rate constants have not been measured previously for DG or FDG in human beings, we cannot compare our work with that of others. However, these constants for DG have been measured with an autoradiographic technique in rats and monkeys. Our values of k_1^* and k_2^* for gray and white matter are lower than values for DG reported by Sokoloff et al [53] in rat brain, whereas the values of k_3^* are very similar (see Table 1). This may imply that FDG has a lower affinity than DG for the facilitated transport system of the capillary membrane but is very similar as a substrate for hexokinase. However, without data for DG in humans, this is only a conjecture. Our values of $k_2^* + k_3^*$ tend to be lower than those found by Kennedy et al [26] from measurements in 2 rhesus monkeys with DG (see Table 1). This supports the hypothesis that differences in the values of k_1^* and k_2^* for DG and FDG result from differences in the chemical form of the two compounds rather than differences in animal species; however, the data are too meager to be conclusive. CMRGlc is somewhat lower in humans than in rats, and lower values of the rate constants would be expected. Also, the spatial resolution of the tomograph used in this study (1.3 cm) produces some averaging of the gray and white matter values, which tends to decrease the gray and increase the white matter values.

Since our values of k* from different gray and white matter structures did not vary significantly when compared to variations of the same structure from one subject to another, we have listed only average values for these two general categories of cerebral tissue. The same result was found for DG in rat brain [53]. The effect of different k* values for substructures of the brain is discussed later in the section titled "Compartmental Model."

Although the activity of glucose-6-phosphatase is reported to be low in mammalian brain [20, 21, 44, 45], it apparently produces a significant hydrolysis of FDG-6-PO_4 to FDG, which is then available for rephosphorylation (k_3^*) or clearance into the blood (k_2^*). Our extension of Sokoloff's model has been derived [23] to include the hydrolysis reaction mediated by the rate constant k_4^* (see Fig 1 and Eq. 23). Sokoloff et al [53] measured the total ^{14}C tissue activity at 17 and 24 hours after injection of DG and, by assuming the blood concentration to be zero, found gray and white matter to have clearance half-times of 7.7 and 9.7 hours, respectively. If we neglect the blood FDG activity in the period from 3 to 14 hours after injection, we also find an average tissue clearance rate of 9.1 hours. This indicates that the data of Sokoloff et al would yield a k_4^* similar to ours if processed in our model.

Our values for k_4^* (gray matter, 0.68%/min, and white matter, 0.58%/min) are in reasonable agreement, although somewhat lower, than the low values of 1% and 0.7% per minute reported from (C-14) DG studies in rats by Hawkins and Miller [19]. They also reported measured values as high as 3.5% per minute. This discrepancy may be because these authors underestimated the initial portion of their "estimated" DG blood curve since they fitted it with a single exponential. We have found in dogs, monkeys, and humans, as Sokoloff et al [53] have noted in rats and Kennedy et al [26] in monkeys, that the plasma curve is best fitted with four exponentials. Gallagher et al [11] have fitted the plasma curve from dogs with three exponentials. The single exponential fit of Hawkins and Miller [19] probably missed the very large early portion of the blood curve. This would cause underestimation of the initial amount of DG supplied to the tissue, so that subsequent DG in the blood would appear to be providing the tissue with major amounts of DG without significant increases in the amount of DG-6-PO_4. This gives the false impression that DG-6-PO_4 is being formed and rapidly removed by hydrolysis.

There now appears to be no question that small amounts of phosphatase are present in cerebral tissue [12, 14, 20, 21, 44, 45, 54] and that if studies are carried out at significantly long times after administration (i.e., $\geq$40 minutes) the hydrolysis of FDG-6-PO_4 to FDG should be taken into account by the model given in Eq. 23. The spatial distribution and specific function of phosphatase in the brain are still not clearly understood [1]. It has been reported that phosphatase is also located in capillary membranes and may be integrally involved in the facilitated transport mechanism for glucose [14, 54].

Our estimated LC value of 0.420 $\pm$ 0.059 (SD) is between the values measured for DG of 0.483 $\pm$ 0.022 (SEM) in rat [53] and 0.344 $\pm$ 0.036 (SEM) in monkey [26]. Our value is considerably higher than the LC of 0.282 estimated by Reivich et al [49] for FDG in the primate. The LC for FDG, however, needs to be directly measured in humans and other primates. The stability of LC must also be determined in various normal and abnormal states.

Turnover Rate of FDG in Tissue

The half-time for turnover of the tissue FDG pool can be approximated by $\ln 2/(k_2^* + k_3^*)$ when k_4^* is small. Our values for white matter in human beings are

Table 5. Rate Constants, Half-Times of Precursor Pool, and Distribution Volume of DG and FDG in Animals and Humans

Determination	$k_2^* + k_3^*$ (min^{-1})		Half-life of Precursor Pool $\ln 2/(k_2^* + k_3^*)$ (min)		Distribution Volume $k_1^*/(k_2^* + k_3^*)$		Whole Brain Average Distribution Volume[a]
	Gray Matter	White Matter	Gray Matter	White Matter	Gray Matter	White Matter	
DG in rat[b] (Sokoloff et al [53])	0.297	0.153	2.39 ± 0.40	4.51 ± 0.90	0.647 ± 0.073	0.516 ± 0.171	0.582
DG in monkey (Kennedy et al [26])	0.347	0.144	2.00	4.81			
FDG in humans[c] (this work)	0.192 ± 0.079	0.154 ± 0.058	4.25 ± 1.78	5.30 ± 2.49	0.593 ± 0.230	0.383 ± 0.137	0.488

[a]Assumes that whole brain is 50% white and 50% gray matter [25].
[b]Error values are *standard error of the mean.*
[c]Error values are *standard deviation of the mean.*

similar to the values from DG in rat and monkey (Table 5). However, our half-time for gray matter in humans is about twice the DG value in rat and monkey (Table 5), which may result from spatial averaging in PCT or from species or chemical differences. Since CMRGlc and blood flow are somewhat lower in man than in rats, lower values for the pool turnover rate in humans are expected.

Compartmental Concentrations of FDG plus FDG-6-PO$_4$

The concentrations shown in Figure 6 of total F-18 activity between FDG and FDG-6-PO$_4$ in tissue as a function of time are typical of our results. These data clearly show that F-18 concentration increases for about 90 minutes and then levels off for both gray and white matter. The shape and ratio of concentrations in each compartment for both gray and white matter are in reasonable agreement with the data of Sokoloff et al [53] for the first 45 minutes over which they report data. Our data show a slower rate of FDG-6-PO$_4$ formation, but this is expected from the lower CMRGlc in humans. The data in Figure 6 and from studies carried out for 5 to 14 hours indicate that the total tissue F-18 activity slowly decreases after 120 minutes, apparently due to hydrolysis of FDG-6-PO$_4$ by phosphatase.

The present data and those of Sokoloff et al [53] are not in good agreement with the data of Hawkins and Miller [19], who reported direct chemical assays of tissue DG and DG-6-PO$_4$ in rat brain. Hawkins and Miller reported that the total tissue activity (DG-6-PO$_4$ and DG plus some small amount—small at times <1 hr—of unknown labeled compound) decreased after 10 minutes. In their data, this was because DG was declining with time, as would be expected, but DG-6-PO$_4$ was constant or decreasing slightly. These authors [19] stated that net phosphorylation of DG ceases after 10 minutes even though significant amounts of DG are present in blood and tissue. As stated before, we believe that Hawkins and Miller have underestimated the early portion of the plasma DG curve, and therefore have significantly overestimated the relative magnitude (i.e., overestimated the rate of dephosphorylation) of DG supplied to tissue at the late times.

Direct chemical assay of FDG-6-PO$_4$ in mouse brain by Gallagher et al [12] showed that total tissue radioactivity increased rapidly for the first few minutes and then remained almost constant for about 1 hour, after which it appeared to decrease slowly. FDG-6-PO$_4$ reached a value of 90 to 95% of total tissue activity in a few minutes and then followed the total tissue activity. Gallagher et al [12] did not show blood curves, so the temporal delivery of FDG to brain is not known. Since the mouse has a higher CMRGlc and CBF and much shorter body circulation time than man, it is not surprising that maximum DG-6-PO$_4$ values were reached much more quickly than in our study. However, this is inconsistent with the data of Sokoloff et al [53] and Hawkins and Miller [19].

In terms of the fractional distribution of tissue radioactivity between FDG and FDG-6-PO$_4$ (see Table 2), our data are in reasonably good agreement with those of Sokoloff et al [53] and Hawkins and Miller [19]. Our values for the early times (<30 minutes) are, however, considerably lower than those of Gallagher et al [12]. The notable difference in their data is that after only a few minutes, about 90% of the tissue activity is in the form of FDG-6-PO$_4$.

Figure 7 shows that the measured fraction of tissue radioactivity due to tissue plasma (or whole blood by Eq. 27) FDG rapidly decreases to a value of about 1.32% and 0.77% at 40 and 80 minutes, respectively. The fractions in terms of whole blood at 40 and 80 minutes are 1.89% and 1.10%, respectively. If FDG were distributed with uniform concentration throughout the brain, then the extravascular FDG would be in a volume about 32 times as large as the

vascular volume. This would imply that at 40 and 80 minutes, the fraction of total tissue radioactivity due to free FDG would be about 60% and 35%, respectively. These values are considerably higher than our calculated values (Table 2, column 6) using the CMRGlc model (Eq. 23) and our measured values of k*s. This indicates that the average extravascular concentration of FDG is lower than the vascular concentration (i.e., the distribution volume or partition coefficient for FDG is less than 1; see Table 5). This is expected, since glucose is transported into the brain by a saturable facilitated mechanism rather than an active mechanism [6, 7, 9, 10, 57] and therefore requires greater plasma than tissue glucose concentrations. These data indicate that the average ratio between the concentration of FDG in brain tissue and that in blood is about 0.51, which is consistent with the model value of 0.49 (distribution volume in Table 5).

Since red cells could be sequestering FDG-6-PO_4, we measured the concentration ratios of RBC to plasma (see Fig 8). This showed that RBCs rapidly equilibrate with plasma FDG (due to the ease with which DG crosses cell membranes [1, 32]), sequester FDG-6-PO_4 very slowly, and have a total F-18 concentration close to that of plasma for a 5-hour period. The slow sequestering rate of RBCs is consistent with their large glucose content and low metabolic rate for glucose [34, 35]. This indicates that the tissue blood radioactivity is not increased or enhanced by a high RBC-plasma concentration ratio.

The distribution volume or partition coefficient between plasma and tissue for FDG is approximately given by $k_1^*/(k_2^* + k_3^*)$ when k_4^* is small. Our values of 0.593 and 0.383 for gray and white matter in humans are lower than the corresponding values of 0.647 and 0.516 for DG in rats (see Table 5). The difference between our values and those of Sokoloff et al [53] arises primarily from our lower values of k_1^* and k_2^* (see Table 1), but the difference is insignificant by a paired t test.

Arterial and Venous Blood Sampling

Sokoloff et al [53] and Reivich et al [48, 49] have used peripheral arterial plasma values of DG and glucose for estimating the cerebral capillary concentration of these substrates. Sokoloff et al [53] reasoned that since the cerebral arteriovenous extraction fraction, (A-V)/A, is small (~5%), the arterial values provide a good estimate of mean capillary concentration. Also, since the glucose values appear in the numerator and the DG values in the denominator, the difference tends to cancel partially (complete cancellation does not occur because the second term in the numerator also contains the plasma DG concentration; see Eqs. 2 and 23). This partial cancellation effect allows a better estimate of the capillary concentrations, since the difference between the systemic and capillary values also partially cancels.

We have likewise reasoned that one could use the venous values from a resting arm or hand. The reported (A-V)/A for glucose in humans of 2 to 5% across a resting arm [2–4] is small, although lower than our measured values of 7.5 ± 0.21% for humans and close to 3.6 ± 0.10% for dogs and monkeys. The reported values [2–4] are somewhat lower than ours because those subjects were fasted for 24 hours. However, a labeled compound is equal to the normal circulating compound only when a steady state or equilibrium is reached. For example, the first-pass extraction of the tracer will be larger than that of the circulating compound if the reverse transport is not equilibrated (see Fig 9). For tracers with slow equilibration times, the initial venous values are substantially lower than arterial values for the tracer. Subsequently, the venous values may even rise above arterial values if the arterial concentration falls rapidly as back-transport is equilibrating (Fig 9). However, after equilibration, the tracer A-V difference will equal the circulating compound A-V difference. In the case of DG, the tracer A-V at steady state will be somewhat lower because LC is below 1.0. Thus, only after sufficient equilibration time will the ratio of venous plasma concentration of glucose to FDG be in good agreement with the ratios of the artery or capillary.

The ratio of the venous to arterial FDG plasma input functions divided by the ratio of the average venous to arterial plasma glucose concentrations is between 0.97 and 1.04 at 30 to 180 minutes, as shown in columns 4 and 7 in Table 3 (the value becomes slightly greater than 1.0 because the LC for FDG in the arm is less than 1.0: Phelps, unpublished data). Thus, venous values of FDG and glucose can be used without a significant loss in accuracy and provide a less traumatic method for determining the cerebral capillary plasma concentrations for calculation of CMRGlc.

We have found, however, that there is significant individual variability between venous and arterial concentrations of FDG at the early times. This is because the time to reach steady state depends to a large extent upon the blood flow in the arm (i.e., the slower the arm blood flow, the longer the time required to reach steady state). Also, when there is low flow (particularly in older patients) in a peripheral vein, it is sometimes difficult to draw the necessary blood samples. To avoid these problems, we now heat the hand of the subject from which venous blood samples are drawn. This arterializes the venous blood, as shown in Figure 10 and Table 4. The high blood flow rate also improves blood sampling. The technique allows one essentially to sample arterial blood without puncturing an artery.

Compartmental Model

Sokoloff et al [53] extensively described the derivation and assumptions of their compartment model. Since our three-compartment model is derived from Sokoloff's, their discussion applies equally well to our model with the exception of our k_4^*-mediated hydrolysis of FDG-6-PO_4 to FDG. The assumptions of the model, error analysis, and optimized experimental design for measurement of CMRGlc have been performed [23].

The rate constants measured in this work are for normal brain tissue, and they will vary not only in abnormal tissue, but also whenever there is a change in CMRGlc. CMRGlc changes by altering the rate constants (the rate constants are not universal constants, but constants for a particular steady-state condition of CMRGlc). Thus, our rate constants are average values for CMRGlc within a normal range, and can be used without much error in the calculated CMRGlc with Eq. 23. Error analysis by Huang et al [23] indicates that the error in CMRGlc by using Eq. 23 and an average set of rate constants is about 10% for the normal range of CMRGlc when tomography is performed between 40 and 150 minutes post injection. As pointed out by Sokoloff et al [53], one must not only use good average estimates of k*s but must also design the measurement protocol to minimize the effects of variations in the rate constants. The magnitude of the k*s which determine the distribution of tracer between compartments as a function of time and the rate at which steady state is reached must be known to optimize the measurement protocol. Initially after injection the terms involving the rate constants are very large, and any error resulting from use of the average values produces significant errors in CMRGlc (see Fig 5). However, 40 to 50 minutes after injection, when a number of half-times of the kinetic processes have occurred and steady-state conditions are approached, the sensitivity to the exact values of the k*s is lowered and CMRGlc can be measured with a minimum error [23].

This type of tracer kinetic model also applies when labeled natural substrates are employed, such as (C-14)- or (C-11)glucose. With the labeled natural substrate one does not have to account for the differences that exist in transport and phosphorylation between a labeled analog and glucose (i.e., LC), but otherwise the modeling approach is the same. The fact that DG is trapped or sequestered in tissue is the key factor which allows accurate analytical modeling and measurement of CMRGlc. The trapping allows one to wait long enough to reduce the sensitivity to exact values of the k*s and for free FDG in tissue to be reduced to a low level. This is difficult, though not impossible, with labeled glucose [46, 47] because the labeled breakdown products of glycolysis (CO_2, pyruvate, and others) rapidly diffuse out of cerebral tissue. Moreover, labeled products from glycolysis in the rest of the body will contaminate the blood activity (i.e., the input function) and diffuse into cerebral tissue, contaminating the tissue data [46].

Labeled natural substrates have an advantage over DG since LC is unity. However, as discussed by Sokoloff et al [53], LC consists of ratios of kinetic constants of DG to glucose (except for one term, ϕ, which is approximately unity [53]); and where different cerebral conditions may change the individual constants, it is likely that the change would occur in the same direction for both DG and glucose, thereby reducing the effect. This has been shown [53] to be true for changes in CMRGlc due to anesthesia and Pa_{CO_2}-induced changes in cerebral blood flow, but it must be further investigated.

The value of LC in this work is estimated by assuming that the average CMRGlc in our normal subject population is equal to the average value for humans in the literature (5.38 mg/min/100 gm). A direct measurement of LC would probably yield a more accurate value. LC is a multiplicative constant in the calculation of CMRGlc, and if better estimates of LC are determined, the values of CMRGlc can be adjusted proportionately. The other variables and procedures are not affected by the uncertainty in LC.

The spatial resolution of PCT does not allow complete delineation of cerebral structures, and therefore the k*s and CMRGlc will exhibit some admixture of gray and white matter [22]. This will produce some underestimation in gray and overestimation in white matter. The largest effect will be in gray matter structures because they tend to be smaller. This effect will also cause some underestimation of LC, but this is expected to be small because it is calculated from the average of gray and white CMRGlc. A major distortion in k*s, LC, and CMRGlc can occur if measurements contain significant amounts of random coincidences, scattered radiation, or errors due to attenuation correction or calibration. The random and scatter coincidences are inherently small in the ECAT [40] and were completely subtracted from the data. Care was taken to minimize errors from attenuation correction (transmission attenuation corrections were used to check the geometric correction method [40]) and calibration; these errors are considered to be very small in this work.

Effects of Disease and Large Variations in CMRGlc and CBF

The use of this model for measurement of CMRGlc in cerebral disease requires some discussion. The ratios of the terms in LC provide a great deal of stability. However, ϕ may be a weak point of LC in certain pathological states. The value of ϕ is unity if all the glucose (not DG) that is phosphorylated is

subsequently metabolized. However, if significant amounts are dephosphorylated, then ϕ will be less than one, LC will increase, and CMRGlc will be overestimated. There might be partial compensation for this effect because the tissue FDG would also be decreased (k_4^* would increase), but it would be variable with time. A ϕ value less than one is unlikely in normal and hypermetabolic states, but it could possibly occur in ischemia if the glycolytic rate is reduced to the point that there is major competition from *dephosphorylation*. This needs to be experimentally determined.

Although the model does not require exact values of k*s, errors in CMRGlc may significantly increase if large variations from the normal range are encountered. While some concern must be expressed for both very high and very low CMRGlc, the most serious problems would probably be encountered in states of low metabolism because they extend from normal to near zero CMRGlc. In ischemia also, the time required to reach steady state would be delayed (producing greater sensitivity to exact k*s), and errors from the use of average rate constants from normal subjects might produce significant errors in CMRGlc (underestimation of CMRGlc). The magnitude of this problem can be investigated by using the tomograph to measure the rate constants in the different disease states of interest. This would yield correct values of k*s for the particular studies and would provide measured ranges of k*s for disease states. These ranges could be used both to determine error bounds from the use of average k*s and to formulate average sets of k*s for high, normal, and low CMRGlc conditions. The appropriate set of k*s could then be chosen from clinical indications, from type of study, or from CMRGlc values determined with the normal average k*s. In the last approach, the initial calculation would be used to select the set of k*s for the high or low range of CMRGlc, and the data simply reprocessed.

In the design of any model for measurement of metabolism, one must be concerned about the effects of blood flow. Initially, the distribution of FDG is highly dependent on cerebral blood flow and volume and the unidirectional transport of FDG into cerebral tissue. However, because of trapping of FDG-6-PO_4, one can wait 40 to 50 minutes for a steady state to be approached in which these factors are usually no longer significant. At this point the measurements reflect CMRGlc. Note in Figures 2 and 3 how, at the early times, the general distribution is somewhat variable. After about 20 minutes the images show a consistent distribution.

Conclusion

We have found that our extension of Sokoloff's model provides reproducible, accurate, and stable measurements of local CMRGlc. The positron tomograph can be used not only for measurement of CMRGlc in human beings, but also to measure the kinetic rate constants for FDG and to validate the model. The studies in Figures 2 through 4 demonstrate the detail and reproducibility of in vivo measurement of LCMRGlc with positron tomography.

We have combined the physiological model, PCT, and FDG into a single-system approach which allows us to measure local CMRGlc in vivo on a routine basis. This capability is an example of a general approach which we refer to as physiological tomography (PT). While the measurements and calculations may be involved, the complexities are necessary only in the initial development of this approach. Once the rate constants were determined, they and the model (Eq. 23) were incorporated into the ECAT system programs. The measurement of CMRGlc requires only intravenous injection of FDG, venous blood sampling, and tomographic imaging. Imaging is started 40 to 50 minutes after injection, when near steady-state conditions have been achieved. The plasma glucose values are determined by the clinical laboratory, and FDG is counted in a well counter. The blood data are entered in the tomograph and the images are converted to units of CMRGlc. Thus, as seen in Figure 11, shortly after scanning, local CMRGlc can be displayed in selected regions of interest (ROI) on the system display. As the ROI is used to survey different locations in the image, the CMRGlc, size, and standard deviation in the region are updated in real time. This system is set up so that studies are now routinely carried out by a nuclear medicine technician.

The ECAT produces a count rate of about 300,000 counts per minute with 1.3 cm resolution at the time of imaging from a 10 mCi injection of FDG. The counting time to achieve the quality of images in this paper—800,000 to 2,000,000 counts per image—is about 2.5 to 6 minutes. If a resolution of 1.7 cm is used, the imaging times are about 1.2 to 3 minutes.

After initial studies with FDG in normal subjects [28, 39, 48, 49], the approach described in this paper was developed and applied to patients with partial epilepsy [29] and patients with a wide variety of different types of focal and diffuse cerebral ischemia [29, 30].

PCT constitutes a noninvasive method for employing tracer methodology for quantitative measurement of cerebral metabolism in living subjects with higher spatial resolution and accuracy than has been possible previously. It allows multiple studies in the same subject and study of time-varying processes in the living subject, without the perturbations and limitations imposed by destructive techniques. The method allows direct investigation of human disorders and avoids the difficulties or impossibility (e.g.,

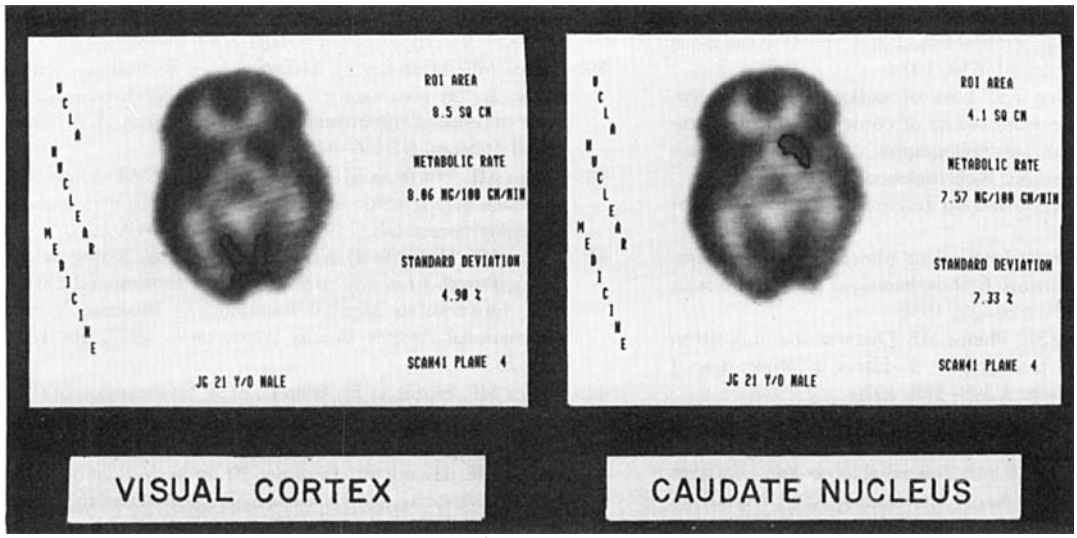

*Fig 11. Region of interest (ROI) extraction of CMRGlc values. Eq. 23, measured values of k*s, and LC are resident in the operating system software of the tomograph so that after plasma values of FDG and glucose are entered, the joy stick of the tomograph can be used to select ROIs for display of the ROI area, CMRGlc, and standard deviation of variation within ROI. As ROI is moved around the image, these parameters are updated in real time.*

schizophrenia) of duplicating human disorders in animals. PT in humans also provides a means of evaluating both the usefulness and the application of data from animal models in the characterization of human disorders.

Supported in part by Department of Energy Contract EY-76-C-03-0012 GEN-12 and National Institutes of Health Grant 7R01-GM-24839.

Presented in part at the Eighth Cerebral Blood Flow Symposium, Copenhagen, Denmark, June 22–30, 1977.

We thank Dr Norman S. MacDonald and his cyclotron staff and Dr Gerald Robinson and his chemistry staff for preparation of the compounds used in this study, and JoAnn Miller, Francine Aguilar, Klear Sideris, and Anthony Ricci for technical assistance. Our thanks are due to Lee Griswold and Hector Pimentel for illustration work. Acknowledgment is given to Dr Alfred Wolf and colleagues, who originally developed and built the targetry for production of FDG.

References

1. Anchors JM, Haggerty DF, Karnovsky ML: Cerebral glucose-6-phosphatase and the movement of 2-deoxy-D-glucose across cell membranes. J Biol Chem 252:7035–7041, 1977
2. Andres R, Baltzan MA, Cadar G, et al: Effect of insulin on carbohydrate metabolism and on potassium in the forearm of man. J Clin Invest 41:108–115, 1962
3. Andres R, Cader G, Zierler K: The quantitatively minor role of carbohydrate in oxidative metabolism by skeletal muscle in intact man in the basal state. Measurements of oxygen and glucose uptake and carbon dioxide and lactate production in the forearm. J Clin Invest 35:671–682, 1956
4. Baltzan MA, Andres R, Cader G, et al: Heterogeneity of forearm metabolism with special references to free fatty acids. J Clin Invest 41:116–125, 1962
5. Bessell EM, Foster AB, Westwood JH: The use of deoxyfluoro-D-glucopyranoses and related compounds in a study of yeast hexokinase specificity. Biochem J 128:199–204, 1972
6. Betz AL, Gilboe DD, Yudilevich D, et al: Kinetics of unidirection glucose transport in the isolated dog brain. Am J Physiol 225:586–592, 1973
7. Buschiazzo PM, Terrell EB, Regen DM: Sugar transport across the blood brain barrier. Am J Physiol 219:1505–1513, 1970
8. Cohen PJ, Alexander SC, Smith TC, et al: Effects of hypoxia and normocarbia on cerebral blood flow and metabolism in conscious man. J Appl Physiol 23:183–189, 1967
9. Culter RWP, Sipe JC: Mediated transport of glucose between blood and brain in the cat. Am J Physiol 220:1182–1186, 1971
10. Fishman RA: Carrier transport of glucose between blood and cerebral spinal fluid. Am J Physiol 206:173–177, 1973
11. Gallagher BM, Ansari A, Atkins H, et al: Radiopharmaceutical XXIII. ^{18}F-labeled glucose metabolism in vivo: tissue distribution and imaging studies in animals. J Nucl Med 18:990–996, 1977
12. Gallagher BM, Fowler JS, Gutterson NI, et al: Metabolic trapping as a principle of radiopharmaceutical design. The factors responsible for the bio-distribution of ^{18}F-2-deoxy-2-fluoro-D-glucose (^{18}FDG). J Nucl Med 19:1154–1161, 1978
13. Goldschmidt S, Light AB: A method of obtaining from veins blood similar to arterial blood in gaseous content. J Biol Chem 64:53–58, 1925
14. Goldstein GG, Wolinsky JS, Csejtey J, et al: Isolation of metabolically active capillaries from rat brain. J Neurochem 25:715–717, 1975
15. Gottstein E, Bernsmeier A, Sedlmeyer I: Der Kohlenhydratstoffwechsel des menschlichen Gehirns. Klin Wochenschr 41:943–948, 1963
16. Greenberg JH, Alavi A, Reivich M, et al: Local cerebral blood volume response to carbon dioxide in man. Circ Res 43:324–331, 1978
17. Grubb RL Jr, Phelps ME, Ter-Pogossian MM: Regional cerebral blood volume in humans. Arch Neurol 28:37–42, 1973

18. Grubb RL Jr, Raichle ME, Eichling JO, et al: The effects of changes in P_aCO_2 on cerebral blood flow and vascular mean transit time. Stroke 5:630–639, 1974
19. Hawkins RA, Miller AL: Loss of radioactive 2-deoxy-D-glucose-6-phosphate from brains of conscious rats. Implications for quantitative autoradiographic determination of regional glucose utilization. Neuroscience 3:251–258, 1978
20. Hers HG: Le Métabolisme du fructose. Brussels, Éditions Arscia, 1957, p 102
21. Hers HG, De Duve C: Le Systeme phosphatasique: repartition de l'activité glucose-6-phosphatasique dans les tissus. Bull Soc Chim Biol 32:20–29, 1950
22. Hoffman EJ, Huang SC, Phelps ME: Quantitation in positron emission computed tomography: 1. Effect of object size. J Comput Assist Tomogr 3:299–308, 1979
23. Huang SC, Phelps ME, Hoffman EJ, et al: Non invasive determination of local cerebral metabolic rate of glucose in normal man with (F18)2-fluoro-2-deoxyglucose and emission computed tomography: theory and results. Am J Physiol (in press)
24. Ido T, Wan CN, Casella V, et al: Labeled 2-deoxy-D-glucose analogs. ^{18}F-labeled 2-deoxy-2-fluoro-D-glucose, 2-deoxy-2-fluoro-D-mannose and ^{14}C-2-deoxy-12-fluoro-D-glucose. J Label Compds Radiopharm 24:174–183, 1978
25. Ingvar DH, Lassen NA: Regional cerebral blood flow. Acta Neurol Scand [Suppl] 24:65–82, 1965
26. Kennedy C, Sokurada O, Shinohara M, et al: Local cerebral glucose utilization in the normal conscious macaque monkey. Ann Neurol 4:293–301, 1978
27. Kuhl DE, Alavi A, Hoffman EJ, et al: Local cerebral blood volume in head-injured patients: determination by emission computed tomography of Tc-^{99m} red cells. J Neurosurg (in press)
28. Kuhl DE, Hoffman EJ, Phelps ME, et al: Design and application of the MARK IV scanning system for radionuclide computed tomography of the brain, in Medical Radionuclide Imaging. Vienna, International Atomic Energy Association, 1977, vol 1, pp 309–320
29. Kuhl DE, Phelps ME, Engel J Jr, et al: Relationship of local cerebral glucose utilization and relative perfusion in stroke and epilepsy: determination by emission computed tomography of (F-18) fluorodeoxyglucose and (N-13) ammonia (abstract). J Comput Assist Tomogr 2:155, 1978
30. Kuhl DE, Phelps ME, Hoffman EJ, et al: Initial clinical experience with 18F-2-deoxy-D-glucose for determination of local cerebral glucose utilization by emission computed tomography. Acta Neurol Scand 56:suppl 64:192–193, 1977
31. Kuhl DE, Reivich M, Alavi A, et al: Local cerebral blood volume determined by three-dimensional reconstruction of radionuclide scan data. Circ Res 36:610–619, 1975
32. Lund-Anderson H, Kjeldsen CS: Uptake of glucose analogues by rat brain cortex slices: membrane transport versus metabolism of 2-deoxy-D-glucose. J Neurochem 29:205–211, 1977
33. Novak P, Goluboff B, Bortin A, et al: Studies of the cerebral circulation and metabolism in congestive heart failure. Circulation 7:724–731, 1953
34. Passow H: Ion and water permeability of the red blood cell, in Bishop C, Surgenor DM (eds): The Red Blood Cell. New York, Academic, 1964, pp 71–145
35. Pennell RB: Composition of normal human red blood cells, in Bishop C, Surgenor DM (eds): The Red Blood Cell. New York, Academic, 1964, pp 29–69
36. Phelps ME: Emission computed tomography. Semin Nucl Med 7:737–765, 1977
37. Phelps ME, Grubb RL Jr, Ter-Pogossian MM: Correlation between P_aCO_2 and regional cerebral blood volume by x-ray fluorescence. J Appl Physiol 35:274–280, 1973
38. Phelps ME, Grubb RL Jr, Ter-Pogossian MM: In vivo regional cerebral blood volume by x-ray fluorescence: validation of method. J Appl Physiol 35:741–747, 1973
39. Phelps ME, Hoffman EJ, Huang SC, et al: Positron tomography: an "in vivo" autoradiographic approach to measurement of cerebral hemodynamics and metabolism. Acta Neurol Scand 56:suppl 64:446–447, 1977
40. Phelps ME, Hoffman EJ, Huang SC, et al: ECAT: a new computerized tomographic imaging system for positron emitting radiopharmaceuticals. J Nucl Med 19:635–647, 1978
41. Phelps ME, Hoffman EJ, Kuhl DE: Physiologic tomography: a new approach to *in vivo* measure of metabolism and physiologic function, in Medical Radionuclide Imaging. Vienna, International Atomic Energy Association, 1977, vol 1, pp 233–253
42. Phelps ME, Hoffman EJ, Selin C, et al: Investigation of (^{18}F)-2-fluoro-2-deoxyglucose for the measure of myocardial glucose metabolism. J Nucl Med 19:1311–1319, 1978
43. Phelps ME, Huang SC, Hoffman EJ, et al: Validation of the noninvasive tomographic measure of regional cerebral glucose metabolism in man with (F-18)-2-fluoro-2-deoxyglucose (abstract). J Comput Assist Tomogr 2:656–657, 1978
44. Prasannan RG, Subrahmanyan D: Effect of insulin on synthesis of glycogen in cerebral cortical slices of alloxan diabetic rats. Endocrinology 82:1–6, 1968
45. Raggi F, Kronfeld DS, Kleiber M: Glucose-6-phosphatase activity in various sheep tissues. Proc Soc Exp Biol Med 105:485–486, 1960
46. Raichle ME, Larson KB, Phelps ME, et al: In vivo measurement of brain glucose transport and metabolism employing glucose-^{11}C. Am J Physiol 228:1936–1948, 1975
47. Raichle ME, Welch MJ, Grubb RL Jr, et al: Measurement of regional substrate utilization rates by emission tomography. Science 199:986–987, 1978
48. Reivich M, Kuhl D, Wolf A, et al: Measurement of local cerebral glucose metabolism in man with ^{18}F-2-fluoro-2-deoxy-D-glucose. Acta Neurol Scand 56:suppl 64:192–193, 1977
49. Reivich M, Kuhl D, Wolf A, et al: The (^{18}F) fluorodeoxyglucose method for the measurement of local cerebral glucose utilization in man. Circ Res 44:127–137, 1979
50. Robinson GD Jr, MacDonald NS, Easton MP, et al: F-18 fluorodeoxyglucose: remote, semi automated production using a compact cyclotron (abstract). J Nucl Med 19:701, 1978
51. Scheinberg P, Stead EA: The cerebral blood flow in male subjects as measured by the nitrous oxide technique. Normal values for blood flow, oxygen utilization, glucose utilization and peripheral resistance, with observations on the effect of tilting and anxiety. J Clin Invest 28:1163–1171, 1949
52. Smith AL, Newfeld GR, Ominsky AJ, et al: Effect of arterial CO_2 tension on cerebral blood flow, mean transit time and vascular volume. J Appl Physiol 31:701–707, 1971
53. Sokoloff L, Reivich M, Kennedy C, et al: The (^{14}C) deoxyglucose method for the measurement of local cerebral glucose utilization: theory, procedure and normal values in the conscious and anesthetized albino rat. J Neurochem 28:897–916, 1977
54. Stephen HR, Sanborn EB: Cytochemical localization of glucose-6-phosphatase activity in the central nervous system of the rat. Brain Res 113:127–146, 1976
55. Takeshita H, Okuda V, Sari A: The effects of ketamine on cerebral circulation and metabolism in man. Anesthesiology 36:69–75, 1972
56. Weiner RS, Cooper PL: The use of "arterialized" blood for the determination of arterial O_2 and CO_2 tensions. J Thorac Surg 30:683–686, 1955
57. Yudilevich DL, DeRose N: Blood-brain transfer of glucose and other molecules measured by lipid indicator dilution. Am J Physiol 220:841–846, 1971